



1 **A comparison of two methods to quantitatively evaluate the effect of**  
2 **below-cloud evaporation on the precipitation isotopic composition in the**  
3 **semi-arid region of the Chinese Loess Plateau**

4 Meng Xing<sup>1,2\*</sup>, Weiguo Liu<sup>1,2,3\*</sup>, Jing Hu<sup>1,2</sup>, Zheng Wang<sup>1,2</sup>

5

6

7 1.State Key Laboratory of Loess and Quaternary Geology, Institute of Earth  
8 Environment, Chinese Academy of Sciences, Xi'an, 710061, China

9 2.CAS Center for Excellence in Quaternary Science and Global Change, Xi'an,  
10 710061, China.

11 3. University of Chinese Academy of Sciences, Beijing, 100049, China

12

13 Corresponding authors:

14 Meng Xing email address: [xingmeng@ieecas.cn](mailto:xingmeng@ieecas.cn)

15 Weiguo Liu email address: [liuwg@loess.llqg.ac.cn](mailto:liuwg@loess.llqg.ac.cn)

16

17

18

19

20

21

22

23

24

25

26

27

28

29

30

31



32 Abstract:

33 Below-cloud evaporation effect could heavily alter the isotope composition of the rain  
34 water as it travels from the saturated environment in the cloud towards the surface,  
35 especially in the arid and semi-arid regions, and accounts for misinterpreting the  
36 isotopic signal. To correctly understand the information contained in the precipitation  
37 isotopes, the first step is to qualitatively analyze the below-cloud processes that the  
38 raindrops have encountered during their falling, and then to quantitatively compute the  
39 below-cloud evaporation ratio of raindrops. Here, based on two-year observations of  
40 precipitation and water vapor isotopes in Xi'an, we systematically evaluated the  
41 variations of precipitation and water vapor isotopes caused by the below-cloud  
42 evaporation effect. The precipitation  $\delta^{18}\text{O}$  and  $\delta^2\text{H}$  values range from -18.2‰ to 8.8‰  
43 and -131.7‰ to 61.2‰, respectively, while the water vapor  $\delta^{18}\text{O}_v$  and  $\delta^2\text{H}_v$  values  
44 range from -29.5‰ to -10.1‰ and -214.9‰ to -63.9‰. Our results suggest that the  
45 equilibrium method could be successfully used to predict the ground-level water vapor  
46 isotopic composition from precipitation isotopes in semi-arid climates, especially for  
47 the winter data. Moreover, by using  $\Delta d\Delta\delta$ -diagram, our data show that evaporation is  
48 the main below-cloud process of raindrops, while snowfall samples retain the initial  
49 cloud signal because of less isotopic exchange between vapor and solid phases. In  
50 terms of meteorological factors, both temperature, relative humidity, and precipitation  
51 amount affect the intensity of below-cloud evaporation. In arid and semi-arid regions,  
52 the below-cloud evaporation ratio computed by the mass conservation equation would  
53 be overestimated relative to the isotopic method, while relative humidity is the most  
54 sensitive parameter in computing the remaining fraction of raindrop mass after  
55 evaporation. In this study, the mean remaining fractions of raindrop mass calculated  
56 by the isotopic method respectively are 69.2%, 74.5%, 85.2%, and 80.8% in spring,  
57 summer, autumn, and winter. The raindrops are weakly evaporated in autumn and  
58 winter, and heavily evaporated in spring and summer. Based on water vapor and  
59 precipitation isotope compositions, we designed a set of effective methods to evaluate  
60 the below-cloud evaporation effect, and this will improve our understanding of the  
61 information contained in the isotopic signals of precipitation.

62  
63  
64  
65  
66  
67



68 **1 Introduction**

69 The hydrogen and oxygen isotopes of precipitation are one of the greatly important  
70 tools to trace the hydrological cycle and climate change (Bowen et al., 2019; Gat, 1996).  
71 For the paleoenvironment, the isotopic signals of precipitation recorded in ice cores  
72 (Thompson et al., 2000; Yao et al., 1996), tree rings (Liu et al., 2004; Liu et al., 2017b),  
73 speleothems (Cai et al., 2010; Tan et al., 2014), and leaf wax of loess-paleosol  
74 deposits (Wang et al., 2018b) and lake sediments (Liu et al., 2017a, 2019) could be  
75 used to reconstruct the information of temperature, precipitation, and hydrological  
76 regimes in geologic history, as it had participated into the formation or growth of these  
77 geological archives. For the modern environment, the isotopic ratios of precipitation  
78 could be used to quantitatively constraint the water vapor contribution from the end-  
79 members of advection (Peng et al., 2011), evaporation (Sun et al., 2020; Wang et al.,  
80 2016a), transpiration (Li et al., 2016a; Zhao et al., 2019), and even anthropogenic  
81 activities (Fiorella et al., 2018; Gorski et al., 2015; Xing et al., 2020), as precipitation  
82 itself is the importantly consisting parts of the water circulation processes. Due to the  
83 limitations in sampling and isotopic fractionation theories, however, there remains  
84 large uncertainty (i.e., the remaining fraction of below-cloud evaporation, the moisture  
85 recycling ratio, water molecules exchange between the droplet and ambient air, etc.)  
86 in deciphering the information contained in precipitation by using hydrogen and oxygen  
87 isotope ratios (Bowen et al., 2019; Yao et al., 2013).

88

89 Chinese Loess Plateau (CLP) is located in the arid and semi-arid areas, where many  
90 studies have suggested that the precipitation isotopic composition has been more or  
91 less impacted by the below-cloud evaporation and surface moisture recycling effects  
92 (Sun et al., 2020; Wan et al., 2018; Zhang and Wang, 2016). Therefore, before we  
93 utilize precipitation stable isotopes to reconstruct the climate changes or to trace the  
94 water vapor sources, first we need to have a set of reliable evaluation methods to  
95 diagnose whether the isotope ratios of precipitation have been distorted by the below-  
96 cloud evaporation effect (Graf et al., 2019; Wang et al., 2016b). Then, we need to  
97 quantitatively evaluate how much of the raindrops have been evaporated during their  
98 falling. Finally, we are able to use the original precipitation isotopes data, which have  
99 been calibrated by the below-cloud evaporation effect, to discuss the regional water  
100 vapor sources or the global hydrological cycle. At present, however, there are many  
101 efforts to do in the first and second steps.

102

103 Over the past decades, to determine whether the hydrometeors have been evaporated



104 during their falling, most studies depend on a second-order isotopic parameter  
105 (Dansgaard, 1964; Jeelani et al., 2018; Li and Garziona, 2017), deuterium excess  
106 (defined as  $d\text{-excess} = \delta^2\text{H} - 8 \times \delta^{18}\text{O}$ ). This parameter is representative of the kinetic  
107 fractionations, since  $^2\text{H}^1\text{H}^{16}\text{O}$  equilibrates faster than  $^1\text{H}_2^{18}\text{O}$  in different phases (Clark  
108 and Fritz, 1997; Dansgaard, 1964). With both the equilibrium and kinetic effects, the  
109 lighter isotopes ( $^1\text{H}$  and  $^{16}\text{O}$ ) of raindrops preferentially equilibrate or diffuse from the  
110 liquid phase to the gas phase during their falling through unsaturated ambient air, while  
111 the non-equilibrium diffusional process would result in a decrease of d-excess in rain  
112 (FISHER, 1991; Merlivat and Jouzel, 1979). Correspondingly, the non-equilibrium  
113 evaporation effect would cause the increase of deuterium excess in the surrounding  
114 water vapor. The slope of the local meteoric water line (LMWL) has also been widely  
115 used as a metric to infer the below-cloud evaporation effect according to the theory of  
116 water isotope equilibrium fractionation (Chakraborty et al., 2016; Putman et al., 2019b;  
117 Wang et al., 2018a), in which the LMWL's slopes approximately equal to 8.0 belonging  
118 to equilibrium fractionation and that is lower than 8.0 pointing to a non-equilibrium  
119 fractionation, such as the re-evaporation of raindrops. Nonetheless, it should be noted  
120 that a change of air masses (Guan et al., 2013), condensation in supersaturation  
121 conditions (Jouzel et al., 2013), and moisture exchange in the cloud and sub-cloud  
122 layer (Graf et al., 2019) also cause largely spatial variation in slopes and d-excess  
123 values (Putman et al., 2019a; Tian et al., 2018). Traditionally, extensive data on the  
124 isotopic content of the condensed phases (e.g., precipitation, snow, ice core, etc.) have  
125 been widely used to study the mechanisms of the atmospheric transport process of  
126 water vapor and the subsequent phase changes in the atmosphere. Inevitably,  
127 important information will lose by using the isotopic composition of the liquid or solid  
128 water samples only. As an improvement, simultaneous observations of water vapor  
129 and precipitation are applied to distinguish these processes and quantify below-cloud  
130 processes. For example, Yu et al. (2015, 2016) used a custom-made sampling device  
131 to collect daily water vapor samples over the Tibetan and Pamir Plateau, and  
132 discussed moisture source impacts on the precipitation isotopes. Using a three-stage  
133 Caltech Active Strand Cloud water Collector (CASCC), Spiegel et al. (2012b, 2012a)  
134 investigated the impact of different processes within clouds, and found that the origin  
135 of the water vapor forming near-surface clouds (fog) is key in determining the temporal  
136 evolution of cloud water isotopes. With the aid of the off-line water vapor sampling  
137 system, Deshpande et al. (2010) analyzed the rain-vapor interaction using stable  
138 isotopes. However, the old water vapor cryogenic trapping technique is time-  
139 consuming (Christner et al., 2018), labor-intensive (Welp et al., 2012), and discrete



140 (Wen et al., 2016), limiting the further examination of the two-phase system.

141

142 In recent years, with the progress in optical laser systems, the relatively portable field-  
143 deployable laser spectroscopic instruments, simultaneously measuring  $^1\text{H}_2^{16}\text{O}$ ,  
144  $^2\text{H}^1\text{H}^{16}\text{O}$ , and  $^1\text{H}_2^{18}\text{O}$  isotopes, allows performing online, autonomous, and long-term  
145 site measurements of the water vapor stable isotope composition (Aemisegger et al.,  
146 2012; Christner et al., 2018). The emergence of this instrument exerts a great impact  
147 on the study of water vapor isotopic composition, leading to a substantially increased  
148 number of observations in near-ground water vapor, while the interpretation of water  
149 vapor isotopic data has the potential to deepen our cognition in water vapor isotopic  
150 variations and fractionation processes during the two-phase transformation (Noone et  
151 al., 2011; Steen-Larsen et al., 2014). Wen et al. (2010) first analyzed the  $d\text{-excess}_{\text{vap}}$   
152 (denotes the  $d$ -excess of water vapor) at hourly temporal resolution in Beijing, China,  
153 and systematically discussed the controls on the isotopic exchange between vapor  
154 and condensed phase. Griffis et al. (2016) used multi-year water vapor and  
155 precipitation stable isotope results to evaluate the water vapor contributions to the  
156 planetary boundary layer from evaporation in Minnesota, United States. Laskar et al.  
157 (2014) and Rangarajan et al. (2017) comprehensively investigated the water vapor  
158 sources and raindrop-vapor interaction in Taipei, and developed a box model to explain  
159 the controlling factors for high and low  $d\text{-excess}_{\text{vap}}$  events in this region. Combined  
160 with observations and numerical simulations of stable isotopes in vapor and rain  
161 impacted by cold fronts, Aemisegger et al. (2015) clearly revealed the importance of  
162 below-cloud processes for improving the simulations. An overview of the increasing  
163 number of available water vapor isotope observations can be found in Wei et al. (2019).  
164 As a creative work, Graf et al. (2019) introduced a new interpretive framework to  
165 directly separate the convoluted influences on the stable isotopic composition of vapor  
166 and precipitation according to the theoretical fractionation processes, especially the  
167 influences of equilibration and below-cloud evaporation, which enables us to  
168 disentangle the governing below-cloud processes in the course of a rainfall. Although  
169 Graf's et al. (2019) work gives us a new guideline to more accurately judge the  
170 raindrops experienced below-cloud evaporation effect, their work was only validated  
171 on a cold frontal rain event of a short period, and hence more works need to do for  
172 proving the general applicability of their framework.

173

174 In order to get the initial signal of precipitation isotopes, it is necessary to quantitatively  
175 assess the impact of below-cloud evaporation on the stable isotopes. The model



176 suggested by Stewart (1975) has been widely used to calculate the below-cloud  
177 evaporation ratio of raindrops, as the raindrops experienced physical processes have  
178 been explicitly described by this isotope-evaporation model (Müller et al., 2017; Sun et  
179 al., 2020; Zhao et al., 2019). Based on Stewart's (1975) work, the remaining fraction  
180 of raindrop mass ( $F_r$ ) after evaporation could be calculated according to the differences  
181 between the stable isotope ratios in collected precipitation near the ground and below  
182 the cloud base (See Data and Methods, section 2.3.2, eq 7). We note that some of  
183 the studies used the mass conservation model of a falling raindrop to calculate  $F_r$  (See  
184 Data and Methods, section 2.3.3, eq 8; Kong et al., 2013; Li et al., 2016; Sun et al.,  
185 2019; Wang et al., 2016b), and some of the works assumed the  $F_r$  is a constant (Müller  
186 et al., 2017), but no work has been reported by using ground-based and cloud-based  
187 observations of water vapor isotopes to calculate the  $F_r$  according to our knowledge.  
188 Due to the numerous uncertainty of the parameters in the mass conservation model,  
189 such as the factors of terminal velocity, the evaporation intensity, and the diameter of  
190 the raindrops, the error propagation will largely raise the deviation of  $F_r$  in the model.  
191 So far, no work has systematically evaluated the differences of  $F_r$  computed by the  
192 observed isotope results and the classical mass conservation model.

193  
194 Here, we have measured the near-ground water vapor isotope composition in Xi'an  
195 city (34.23°N, 108.88°E), Shaanxi province, located in the CLP, for 2 years, while  
196 collecting 141 precipitation samples (including event-based snowfall samples). The  
197 objectives of this study are to: 1. test the applicability of the  $\Delta d\Delta\delta$ -diagram suggested  
198 by Graf et al. (2019) when it is used to diagnose the below-cloud processes for our  
199 dataset; 2. compare the differences of raindrops below-cloud evaporation ratio  
200 calculated by the observed ground-based water vapor isotope composition and the  
201 mass conservation model; 3. understand the role of main meteorological factors, such  
202 as temperature, relative humidity (RH), and precipitation amount, on the below-cloud  
203 evaporation effect, and the seasonal variations of below-cloud evaporation ratio in CLP.  
204 With the advantages of the paired observations of the vapor and precipitation in stable  
205 isotopes near the ground level, this study will provide a new set of methods to  
206 determine the below-cloud evaporation effect qualitatively. Meanwhile, combined with  
207 quantitative calculation, our insight into the below-cloud evaporation effect on the  
208 isotopic composition of precipitation in arid and semi-arid areas would be deepened  
209 and strengthened.

210

211 **2 Data and methods**



## 2.1 Sampling site

As the capital city of Shaanxi province and the largest city in northwest China, Xi'an is located on the Guanzhong Plain on the southern edge of the CLP at an average elevation of 400 m. The city is located in a semi-arid to arid region and is representative of most cities in the north and northwest of China (e.g., Lanzhou and Xining city, Fig. 1). The mean annual precipitation is 573.7mm, and the mean annual evaporation is 426.6mm from 1951 to 2008 year (Wu et al., 2013). The notable below-cloud evaporation effect has been reported by many studies in this area (Sun et al., 2020; Wan et al., 2018; Zhu et al., 2016).

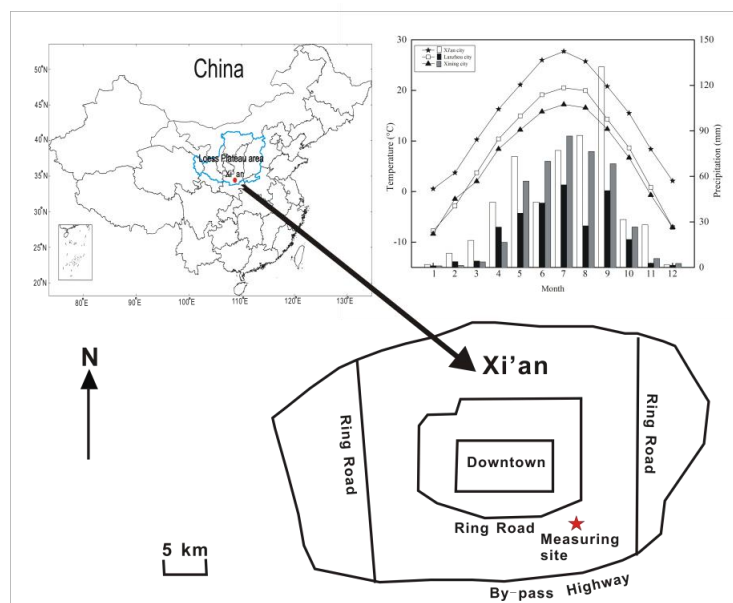


Figure 1 Average monthly variations of temperature and precipitation in Xi'an, Lanzhou, and Xining during 2010-2015. Location of the sampling site in the Yanta Zone, 9 km SE of downtown Xi'an. Water vapor samples are taken on the seventh floor of a twelve-story building, about 30 m above ground level. Precipitation samples are collected on the top floor, 1 m above ground level.

The water vapor in-situ measurement is located in a residential area, approximately 10 km southeast to downtown of Xi'an city (Fig. 1). The atmospheric water vapor isotopic composition was observed from 1 January 2016 to 31 December 2017 on the seventh floor of the Institute of Earth and Environment, Chinese Academy of Sciences, about 30 m above ground level. The rainfall or snowfall collector was placed on the rooftop of the buildings (1 m above the floor of the roof).



## 249 2.2 Sampling and isotopic measurement

250 Rainfall and snowfall samples were collected manually from the beginning of each  
251 precipitation event using a polyethylene collector (700 mm × 450 mm × 170 mm) and  
252 the volume was measured using a graduated flask. Before being used, the collector  
253 was cleaned with soap and water, rinsed with deionized water, and then dried. When  
254 the precipitation events end, the collector was quickly taken back to minimize water  
255 evaporation. Rainfall samples were immediately poured into a 100 ml polyethylene  
256 bottle. The snowfall samples were melted at room temperature in a closed plastic bag  
257 after collection, and then immediately poured into a 100 ml polyethylene bottle. After  
258 collection, samples were filtered through 0.40- $\mu$ m polycarbonate membranes. About  
259 a 2 ml of each filtrate was transferred into a sample vial, and stored at  $-4^{\circ}\text{C}$  until being  
260 measured. Of the 141 samples, during the two-year sampling campaigns, we collected  
261 130 rainfall and 11 snowfall samples (Table S1).

262  
263 In all cases, the data are reported in the standard delta notation ( $\delta$ ), i.e., the per mil  
264 ( $\text{‰}$ ) deviation from Vienna Standard Mean Ocean Water according to,  $\delta =$   
265  $(R_{\text{sample}}/R_{\text{reference}} - 1) \times 1000$ , where R is the isotope ratio of the heavy and light isotope  
266 (e.g.,  $^{18}\text{O}/^{16}\text{O}$ ) in the sample and the reference.

267  
268 The precipitation samples were measured by Picarro L2130-i wavelength-scanned  
269 cavity ring-down spectrometer at a high-precision model. Every isotopic standard or  
270 sample was injected sequentially 8 times using a 5  $\mu\text{L}$  syringe, and then the arithmetic  
271 average of the last 3 injections was accepted as the final result. The precision is better  
272 than 0.2 $\text{‰}$  and 1.0 $\text{‰}$  for  $\delta^{18}\text{O}$  and  $\delta^2\text{H}$ , respectively. All the samples were calibrated  
273 by three laboratory standards, while the  $\delta^{18}\text{O}$  and  $\delta^2\text{H}$  true values of the three  
274 laboratory standards (Laboratory Standard-1 (LS-1):  $\delta^{18}\text{O} = +0.3\text{‰}$ ,  $\delta^2\text{H} = -0.4\text{‰}$ ;  
275 Laboratory Standard-2 (LS-2):  $\delta^{18}\text{O} = -8.8\text{‰}$ ,  $\delta^2\text{H} = -64.8\text{‰}$ ; Laboratory Standard-3  
276 (LS-3):  $\delta^{18}\text{O} = -24.5\text{‰}$ ,  $\delta^2\text{H} = -189.1\text{‰}$ ) are calibrated to the scale of two international  
277 standard material VSMOW-GISP, with a precision of  $\pm 0.2\text{‰}$  and  $\pm 1.0\text{‰}$ , for  $\delta^{18}\text{O}$  and  
278  $\delta^2\text{H}$ , respectively.

279  
280 Atmospheric water vapor  $\delta^{18}\text{O}_v$  and  $\delta^2\text{H}_v$  were also measured by Picarro L2130-i (serial  
281 number HIDS 2104), but at a liquid-vapor dual model. The inlet of the gas-phase  
282 instrument is connected to the vapor source through an external solenoid valve when  
283 measuring vapor samples. This valve can switch the input of the instrument from the  
284 vapor sample to dry gas. The instrument is connected to dry gas prior to being



285 connected to the evaporator for measuring liquid water standards so that any traces of  
286 the water vapor sample are removed from the measurement cell. The standards are  
287 injected into the evaporator and measured by a CTC Analytics autosampler, PAL HTC-  
288 xt (Leap Technologies, Carrboro, NC, USA). The atmospheric water vapor is pumped  
289 through a 2m stainless-steel tube (1/8 inch) using a diaphragm pump at the speed of  
290 4 L min<sup>-1</sup> and detected by the laser spectrometer. The outside length of the stainless-  
291 steel tube is about 0.5m, and the inside length is about 1.5m. We covered the stainless-  
292 steel tube with a heating tape maintained at 60°C to prevent water vapor from  
293 condensing in the stainless-steel tube. The air intake was protected with a shield to  
294 prevent rainwater from entering the sample line and direct sunlight.

295  
296 The raw water vapor  $\delta^{18}\text{O}_v$  and  $\delta^2\text{H}_v$  data were obtained approximately at 1 Hz and  
297 then block-averaged into 24 h intervals. As the main usage of this instrument is to  
298 measure the liquid water samples in our laboratory, it is used to monitor the water  
299 vapor isotopes in its spare time. Thus, the data gaps represent the instrument is in  
300 liquid samples measuring status or maintenance. The daily average of water vapor  
301 isotopic composition is from 8:00 - 20:00 UTC (0:00 – 24:00 for local time). The  
302 average intra-day variability of water vapor isotopic composition is less than 1.2‰ for  
303  $\delta^{18}\text{O}$  and 8.4‰ for  $\delta^2\text{H}$  for two-year data, respectively, and on the precipitation day is  
304 1.4‰ for  $\delta^{18}\text{O}$  and 10.5‰ for  $\delta^2\text{H}$ , respectively.

305  
306 The hourly meteorological data, such as temperature and RH in Xi'an, are reported by  
307 the China meteorological administration, and can be downloaded from the website of  
308 <http://www.weather.com.cn/>. The meteorological station is about 10 km to the north of  
309 our sampling site.

310  
311 Here, we need to note the different sampling frequencies between Graf's et al., (2019)  
312 and our study. To explicitly capture the below-cloud processes of the droplet, Graf's et  
313 al., (2019) study used the intra-event samples, which clearly record the equilibration,  
314 evaporation, and cloud signal on the  $\Delta d\Delta\delta$ -diagram. Particularly, the below-cloud  
315 evaporation effect does not accompany the entire rainfall process, for example, in the  
316 pre-frontal phase, the rain intensity and relative humidity are lower than in the post-  
317 frontal period, which causes the raindrops to be more strongly affected by below-cloud  
318 processes (Graf et al., 2019). In this study, we aim to quantitatively evaluate the  
319 evaporated degree of droplets in a single rain event, and compare the results of two  
320 different methods for calculating the remaining fraction of raindrop mass after



321 evaporation. The per-event isotopic composition of precipitation is an integrated,  
322 mass-weighted average of the composition of all drops contained in a sample (Graf et  
323 al., 2019). The processes that act on a single drop are thus directly relevant for bulk  
324 precipitation. In the per-event sample, the offset between the precipitation equilibrated  
325 isotope ratios and the simultaneously observed isotope ratios of surface vapor can aid  
326 in inferring the below-cloud processes (Conroy et al., 2016). Hence, we chose the per-  
327 event samples as our study objects. Note that, the per-event samples whose isotopic  
328 results do not project on the fourth quadrant of  $\Delta d\Delta\delta$ -diagram, do not indicate the  
329 absence of below-cloud evaporation. It rather is an indication that the equilibration or  
330 the cloud isotopic signals dominate the mass-weighted isotopic composition of all  
331 drops.

332

### 333 2.3 Water vapor isotopic data calibration

334 Due to the isotopic measurements of the cavity ringdown spectrometer with water  
335 vapor concentration effect as outlined by some studies (e.g., Bastrikov et al., 2014;  
336 Benetti et al., 2014; Steen-Larsen et al., 2013), it is important to determine the  
337 humidity-isotope calibration response function. Because we did not have the  
338 Standards Delivery Module (Picarro) system or equivalent, the humidity calibration is  
339 based on data obtained from discrete injections of three known liquid standards with a  
340 PAL autosampler and the Picarro vaporizer unit (Benetti et al., 2014; Noone et al.,  
341 2013). The analyzer is programmed to perform a self-calibration after every 24 hours  
342 of ambient air measurement using an autosampler to inject liquid standards for  
343 producing different humidity. Injections were arranged at humidity levels near 3000,  
344 5000, 8000, 10000, 15000, 20000, 25000, and 30000 ppm. Each reference sample is  
345 measured continuously for 8 times at one humidity level, and the last 3 times results  
346 were used to calculate the average to be recognized as the  $\delta$ -value at the measured  
347 humidity. The humidity correction is the difference between the  $\delta$ -value at the  
348 measurement humidity and the  $\delta$ -value at a reference value taken as humidity = 20000  
349 ppm. The best fit was reached with an exponential function for  $\delta^{18}\text{O}_v$  and a linear  
350 function for  $\delta^2\text{H}_v$  (Fig. S1a and S1b). The isotopic measurements of ambient air  $\delta^{18}\text{O}_v$   
351 samples were corrected for humidity effects using:

$$352 \delta^{18}\text{O}_{\text{humidity calibration}} = \delta^{18}\text{O}_{\text{measured}} - (-4.91 \times e^{(-3.51 \times \text{Measured humidity})}) \quad (\text{eq 1})$$

353 and for ambient air  $\delta^2\text{H}_v$  humidity correction using:

$$354 \delta^2\text{H}_{\text{humidity calibration}} = \delta^2\text{H}_{\text{measured}} - (0.0001 \times \text{Measured humidity} - 1.86) \quad (\text{eq 2})$$



355 where  $\delta_{\text{humidity calibration}}$  is the calibrated data for water vapor stable isotope;  $\delta_{\text{measured}}$  is  
356 the raw, measured data before calibration; and measured humidity is the  
357 corresponding humidity at the time of measurement.

358 To calibrate the measured water vapor isotopic composition to the VSMOW-GISP  
359 scale, three known-value laboratory standards have been used in the conversion,  
360 while these standards were measured in 24 h intervals to correct for instrument drifts.  
361 The detailed post-calibration procedure is given in Xing et al. (2020). The  $1\sigma$  estimated  
362 total uncertainties are from 2.1 to 12.4 ‰ for  $\delta^2\text{H}_v$ , 0.4 to 1.7 ‰ for  $\delta^{18}\text{O}_v$ , and 3.8 to  
363 18.4 ‰ for d-excess<sub>v</sub>, over the range of humidity from 30000 to 3000 ppm on a 10-  
364 minutes average through the approach using a Monte Carlo method.

365

#### 366 **2.4 The representative of the data**

367 During the two-year study, we collected the precipitation samples for each event.  
368 Precipitation samples are generally collected from the beginning of the rainfall to the  
369 end. If the rainfall event exceeds 24 hours, we replace a sample collector at 8 am as  
370 a new precipitation sample. For the observation of water vapor isotopic composition, it  
371 has been done in the instrument's spare time, that is when the instrument is not on  
372 liquid water samples testing mission or maintaining status. In 2 years, a total of 514  
373 days of water vapor isotopic composition were carried out, of which 100 precipitation  
374 samples have corresponding daily average water vapor isotopic results. In this study,  
375 the precipitation events mainly occurred in summer and autumn, and less in winter and  
376 spring. The rainfall amount accounted for more than 70% of the annual rainfall in  
377 summer and autumn (Fig. S2). This is consistent with the multi-year average  
378 precipitation distribution in Xi'an (Fig. 1). Therefore, the samples we collected are  
379 representative of the precipitation characteristics of this region.

380

#### 381 **2.5 Analytical methods**

##### 382 **2.5.1 $\Delta d\Delta\delta$ -diagram**

383 As the raindrop is falling from the cloud base to the ground, it continuously exchanges  
384 with the surrounding vapor, but may lead to net loss as evaporation. However, this  
385 process is very hard to be quantified by observation. Using stable water isotopes, Graf  
386 et al. (2019) introduced a  $\Delta d\Delta\delta$ -diagram to diagnose below-cloud processes and their  
387 effects on the isotopic composition of vapor and rain since equilibration and  
388 evaporation are two various below-cloud processes and lead to different directions in  
389 the two-dimensional phase space of the  $\Delta d\Delta\delta$ -diagram. Here, the differences of  
390 isotopic composition of equilibrium vapor ( $\delta^{18}\text{O}_{\text{pv-eq}}$ , d-excess<sub>pv-eq</sub>) from precipitation



391 samples relative to the observed ground-based water vapor ( $\delta^{18}\text{O}_{\text{gr-v}}$ ,  $\text{d-excess}_{\text{gr-v}}$ ) can  
392 be expressed as:

$$393 \quad \Delta\delta = \bar{\delta}_{\text{pv-eq}} - \bar{\delta}_{\text{gr-v}} \quad (\text{eq3})$$

$$394 \quad \Delta\text{d-excess}_v = \text{d-excess}_{\text{pv-eq}} - \text{d-excess}_{\text{gr-v}} \quad (\text{eq4})$$

395 where  $\bar{\delta}_{\text{pv-eq}}$  and  $\bar{\delta}_{\text{gr-v}}$  are the  $\delta^2\text{H}$  ( $\delta^{18}\text{O}$ ) of water vapor below the cloud base and near  
396 the ground, respectively, and  $\text{d-excess}_{\text{pv-eq}}$  and  $\text{d-excess}_{\text{gr-v}}$  are d-excess values of  
397 water vapor below the cloud base and near the ground, respectively.

398

399 To calculate the water vapor isotopic composition below the cloud base, we  
400 hypothesize the constant exchange of water molecules between the liquid and the  
401 vapor phases during the falling of raindrops, and the isotopic compositions reach  
402 towards equilibrium in the two phases during the processes. In the equilibrium state,  
403 the isotopic fractionation between the liquid and vapor phases follows a temperature-  
404 dependent factor:

$$405 \quad \alpha = \frac{R_{\text{pv-eq}}}{R_p} \quad (\text{eq5})$$

406 where  $R_{\text{pv-eq}}$  is the water vapor isotope ratio between heavy and light isotopes ( $^2\text{H}/^1\text{H}$   
407 and  $^{18}\text{O}/^{16}\text{O}$ ),  $R_p$  is the isotope ratio in precipitation, and  $\alpha$  is a temperature-dependent  
408 equilibrium fractionation factor. Here, when the temperature is greater than  $0^\circ\text{C}$ , we  
409 use the equation of Horita and Wesolowski (1994) to calculate  $^2\alpha$  and  $^{18}\alpha$ , when the  
410 temperature is below  $0^\circ\text{C}$ , the equilibrium fractionation factor proposed by Ellehoj et  
411 al. (2013) is used.

412

413 The above equation can be converted into  $\delta$ -notation as:

$$414 \quad \bar{\delta}_{\text{pv-eq}} = \frac{1}{\alpha} (\bar{\delta}_p + 1000) - 1000 \quad (\text{eq6})$$

415 where  $\bar{\delta}_p$  is the isotope ratio in precipitation.

416

### 417 **2.5.2 Below-cloud evaporation calculated by isotope**

418 Stewart (1975) suggested the falling raindrop isotopic fractionation of evaporation  
419 could be calculated according to the fraction of raindrop mass remained after  
420 evaporation:

$$421 \quad \Delta\delta = \bar{\delta}_p - \bar{\delta}_{\text{zp-eq}} = \left(1 - \frac{Y}{\alpha}\right) (F_{\text{iso}}^\beta - 1) \quad (\text{eq7})$$

422 where  $\bar{\delta}_p$  and  $\bar{\delta}_{\text{zp-eq}}$  are precipitation isotope ratio near the ground and below the cloud  
423 base, respectively;  $F_{\text{iso}}$  is the remaining fraction of raindrop mass after evaporation



424 (hereafter, the remaining fraction of raindrop mass calculated by this method is  
425 denoted as  $F_{\text{iso}}$ );  $\alpha$  is equilibrium fractionation factor for hydrogen and oxygen isotopes;  
426 the parameters of  $\gamma$  and  $\beta$  is defined by Stewart (1975). For the detailed calculation  
427 processes, please refer to the supplemental material (Appendix A), or Wang et al.  
428 (2016b), Salamalikis (2016), Graf et al. (2019), and Sun et al. (2020).

429

### 430 **2.5.3 Below-cloud evaporation calculated by mass conservation model**

431 Before the advent of the laser-based spectrometer, the water vapor isotopic  
432 composition measurement is labor-intensive and time-consuming, generally using the  
433 custom-made cold trap to collect. Normally, its observation is not a routine option.  
434 Therefore, to correct the measured  $\delta/d$ -excess in precipitation (eq7) for the effect of  
435 below-cloud evaporation (Kong et al., 2013; Li et al., 2016a; Zhao et al., 2019) or study  
436 the differences and controls on  $\delta/d$ -excess in precipitation caused by the below-cloud  
437 evaporation (Wang et al., 2016b), the Stewart (1975) model have been widely used.  
438 In the model, the parameter of the remaining fraction of the water-drop mass is variable  
439 and decisive (eq 8), and can be calculated by the law of conservation of mass  
440 (hereafter, the remaining fraction of raindrop mass calculated by this method is  
441 denoted as  $F_{\text{raindrop}}$ ),

$$442 \quad F_{\text{raindrop}} = \frac{m_{\text{end}}}{m_{\text{end}} + m_{\text{ev}}} \quad (\text{eq8})$$

443 Here, the mass of the reaching ground raindrop after evaporation is  $m_{\text{end}}$  and the  
444 evaporated raindrop mass is  $m_{\text{ev}}$ . The parameter of  $m_{\text{ev}}$  is composed of the evaporation  
445 rate and fall time of the drop. Kinzer and Gunn (1951) and Best (1950a) have  
446 parameterized these two variables, respectively. For the detailed calculation  
447 processes, please refer to the supplemental material (Appendix B), or Wang et al.  
448 (2016b), Sun et al. (2020), Kong et al. (2013), and Salamalikis (2016).

449

450 Due to the intrinsic limitations of Stewart's model, which is a mixing model between  
451 the starting and the final isotopic composition, it assumes a homogenous sub-cloud  
452 layer in terms of temperature and humidity (Salamalikis et al., 2016). Here, considering  
453 the location of our study site, we reasonably assume that precipitation forms close to  
454 the average cloud base at about the 850 hPa (~1500 m) isobaric level (Kong et al.,  
455 2013; Li et al., 2016a; Salamalikis et al., 2016). The cloud base temperature and RH  
456 were obtained from the moist adiabatic ascent of an air parcel from the surface with  
457 initially measured temperature and RH (Appendix A). It is worth noting that the results  
458 may be affected by errors originating from assumed cloud base heights and calculated  
459 vertical profiles of temperature and RH. In the future, the pieces of evidence from direct



460 measurement of cloud base heights, temperature, and RH from radiosondes or aircraft  
461 will validate the assumed below-cloud profiles presented here.

462

463 Now, with the emergence of a laser-based spectrometer, high-precision, high-  
464 resolution water vapor isotopic composition measurement is becoming easier, and  
465 thus the evaluation of below-cloud evaporation is becoming more direct. However, little  
466 work has systematically evaluated the differences of  $F_r$  computed by different methods.  
467 Here, we respectively used the isotope and mass conservation methods to calculate  
468 the  $F_r$ , and compared their differences.

469

#### 470 **2.5.4 Statistical Analysis**

471 To compare the difference of the below-cloud evaporation calculated by the two  
472 methods, the independent t-test was performed on SPSS 13.0 (SPSS Inc., Chicago,  
473 US). A significant statistical difference was set at  $p < 0.05$ .

474

### 475 **3 Results and discussion**

#### 476 **3.1 Relationship between water vapor and precipitation isotopic ratios**

477 Influenced by the below-cloud evaporation, the slope of the local meteoric water line  
478 (LMWL) would be lower than 8, the precipitation isotopic composition become more  
479 positive, the d-excess of precipitation would be less than 10, and the equilibrium  
480 calculated water vapor isotopic composition would be more positive than the observed  
481 one. As shown in Figure 2, the LMWL is:  $\delta^2\text{H}_p = 7.0 \times \delta^{18}\text{O}_p + 3.0$  based on event  
482 precipitation isotopic composition, and the local water vapor line (LWVL) is:  
483  $\delta^2\text{H}_v = 7.6 \times \delta^{18}\text{O}_v + 10.0$  based on daily water vapor isotopic composition. Both the slope  
484 and intercept of LMWL are lower than the Global Meteoric Water Line (GMWL) which  
485 are 8.0 and 10.0 (Dansgaard, 1964; Gat, 1996), respectively, indicating the potentially  
486 significant effect of below-cloud evaporation on precipitation (Froehlich et al., 2008). In  
487 general, the slopes of the meteoric water lines are indicative of kinetic processes  
488 superimposed on the equilibrium fractionation, and the little lower slope of LWVL  
489 (slope=7.6) than the expected equilibrium fractionation (slope=8.0) may also relate to  
490 the increasing influence of kinetic processes (Rangarajan et al., 2017).

491

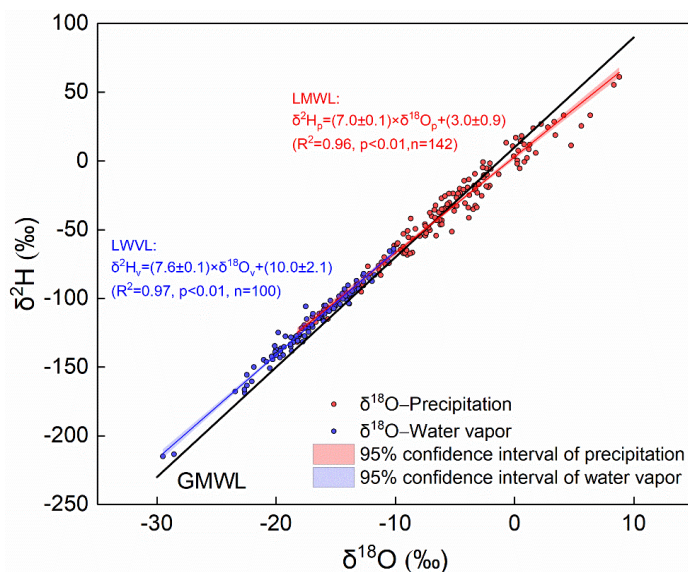
492

493

494

495

496



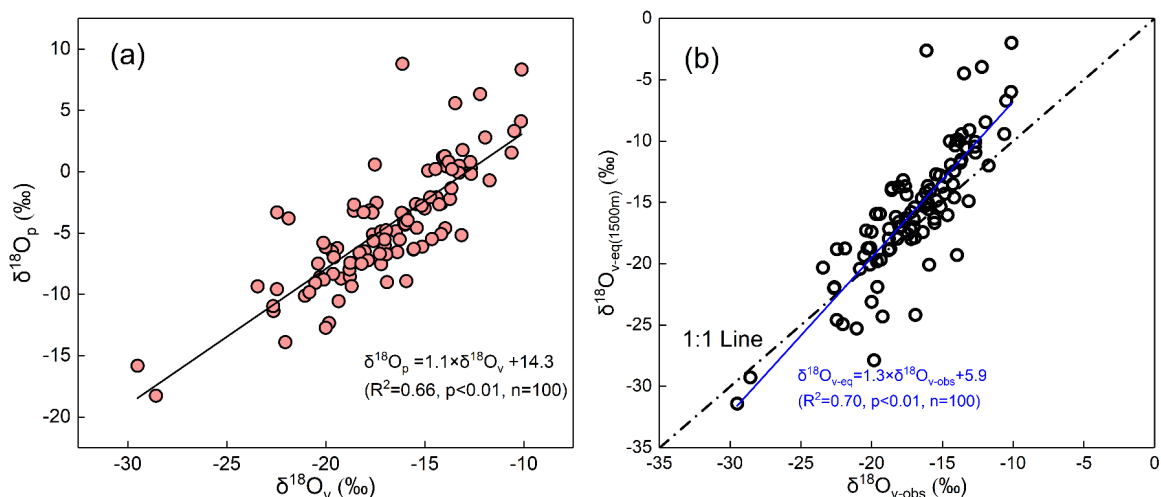
497 Figure 2 Local meteoric water line (LMWL) and Local water vapor line (LMVL) in Xi'an.

498

499 Besides, we note that the water vapor and precipitation isotopic composition basically  
500 distribute in different ranges, and the water vapor isotopic composition is generally  
501 more negative than the precipitation isotopic composition (Fig. 2). According to the  
502 classical isotopic fractionation theory, the heavier isotopes preferentially condense into  
503 the liquid phase resulting in the precipitation isotopic ratios more positive than the  
504 corresponding water vapor during the precipitation process (Dansgaard, 1964). Hence,  
505 the perfect distribution characteristics of water vapor and precipitation on the  $\delta^{18}\text{O}$ - $\delta^2\text{H}$   
506 plot would make us suppose that the precipitation and water vapor isotopic  
507 composition are in or close to equilibrium in this study site. To validate our assumption,  
508 we plot the relationship between the per-event precipitation and the corresponding  
509 day's water vapor isotopic compositions in Figure 3a, as expected they show a  
510 significant positive correlation ( $R^2=0.66$ ,  $p<0.01$ ). The water vapor isotopic composition  
511 can explain above 60% of the variation of precipitation isotopic composition. Further,  
512 we use the measured precipitation isotopic composition to deduce the water vapor  
513 isotopic composition at the cloud base (1500m) according to the liquid-vapor  
514 equilibrium isotope fractionation, and compare it with the observed near-ground water  
515 vapor isotopic composition. As expected, the scatterplot of the observed  $\delta^{18}\text{O}_v$  against  
516 the deduced  $\delta^{18}\text{O}_{v\text{-eq}(1500\text{m})}$  also presents a significantly positive relationship, and the  
517 correlation coefficient increases by 4% (Fig. 3b).

518

519



520 Figure 3 Relationship between  $\delta^{18}\text{O}_p$  of precipitation and  $\delta^{18}\text{O}_v$  of water vapor in Xian (a); and  
521 relationship between the equilibrium computed 1500m  $\delta^{18}\text{O}_v$  based on the precipitation isotopic  
522 composition and the near ground observed  $\delta^{18}\text{O}_v$  (b). The dash-dot line in (b) stands for the 1:1  
523 line, and the blue line represents the regression line of the data.

524

525 The reasonable agreement of  $\delta^{18}\text{O}$  between observed water vapor and equilibrium  
526 prediction has been reported by Jacob and Sonntag (1991), Welp et al. (2008), and  
527 Wen et al. (2010), however, they postulated the different relationship underlying the  
528  $\delta^{18}\text{O}_v$  and  $\delta^{18}\text{O}_{pv\text{-}eq}$ . Jacob and Sonntag (1991) suggested that the water vapor isotopic  
529 composition is possible to be deduced from the corresponding precipitation isotopic  
530 composition, but Wen et al. (2010) speculated that the equilibrium method cannot  
531 accurately predict the ground-level water vapor isotopic composition in arid and  
532 semiarid climates because of two monthly equilibrated precipitation values deviating  
533 the observed water vapor values. Here, with two-year continuous observation, the  
534 mean difference between the  $\delta^{18}\text{O}_{v\text{-}obs}$  and  $\delta^{18}\text{O}_{v\text{-}eq(1500m)}$  is  $-1.1\text{‰}$  for  $\delta^{18}\text{O}$ ,  $-8.1\text{‰}$  for  
535  $\delta^2\text{H}$ , and  $0.7\text{‰}$  for d-excess, and our results indicate that it is possible to derive the  
536 isotope composition of atmospheric water vapor based on that of the precipitation in  
537 the semi-arid area. It is worth noting that we do not propose to extract the water vapor  
538 isotope time series from precipitation data. Because, in dry regions of the world,  
539 precipitation events are rare so deriving vapor isotopes from precipitation can be very  
540 misleading. No data is available for the sometimes long dry spells without precipitation.  
541 These periods are likely to exhibit very special vapor isotope signals about which no  
542 information can be gained from precipitation data.

543



544 In addition, we also noted that the equilibrium calculated  $\delta^{18}\text{O}_{\text{v-eq}(1500\text{m})}$  is relatively more  
545 positive than the  $\delta^{18}\text{O}_{\text{v-obs}}$  (Fig. 3b). In theory, the water vapor isotopic composition  
546 decreases with altitude (Deshpande et al., 2010; Salmon et al., 2019). However, due  
547 to the CLP belonging to the semi-arid area, the raindrops are likely to experience  
548 evaporation in the unsaturated. Therefore, the positively equilibrated  $\delta^{18}\text{O}_{\text{v-eq}(1500\text{m})}$  is  
549 caused by the kinetic fractionation in low relative humidity, and this also makes the  
550  $\delta^{18}\text{O}_{\text{v-eq}}-\delta^{18}\text{O}_{\text{v-obs}}$  points deviate from the 1:1 line.

551

### 552 **3.2 Below-cloud processes indicated by $\Delta d\Delta\delta$ -diagram**

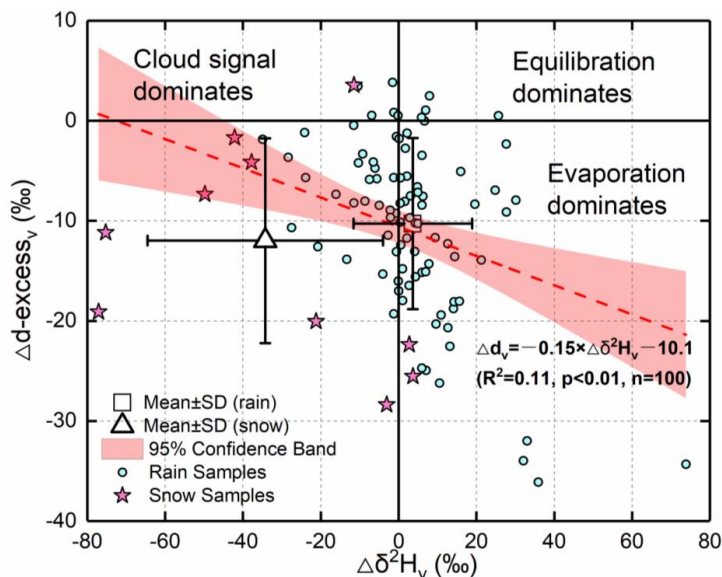
553 Traditionally, to qualitatively assess the below-cloud evaporation of raindrops, the  
554 value of  $d\text{-excess}_p$  is a benchmark, as the isotopically kinetic fractionation will cause  
555  $d\text{-excess}_p$  to deviate from 0‰, which is a theoretical value under vapor-liquid  
556 equilibrium fractionation (Gat, 1996). The global mean value of 10‰ for the  $d\text{-excess}$   
557 in precipitation indicates that evaporation is in general a non-equilibrium process.  
558 Normally, below-cloud evaporation will move  $d\text{-excess}_p$  below 10‰, and in comparison,  
559 mixing with the recycled water vapor from surface evaporation and plant transpiration  
560 will bring  $d\text{-excess}_p$  above 10‰ (Craig, 1961; Dansgaard, 1964). Kinetic (non-  
561 equilibrium fractionation) is due to the differences in diffusivities of the individual water  
562 molecules. Therefore, during the moisture transportation, the water vapor  $d\text{-excess}$   
563 may be modified, and this enhances the uncertainty to gauge the below-cloud  
564 evaporation process by solely using  $d\text{-excess}_p$ . In contrast, the  $\Delta d\Delta\delta$ -diagram  
565 introduced by Graf et al. (2019) provides richer information on the below-cloud  
566 processes.

567

568 By projecting our data on the  $\Delta d\Delta\delta$  plot, the evaporation, equilibration, and non-  
569 exchange (e.g., a snowfall event, or a transition from rain to snow with a stronger cloud  
570 signal) processes could be clearly differentiated (Fig. 4). It is apparent from Fig. 4, that  
571 most of the precipitation samples are located in the fourth quadrant, indicating that  
572 evaporation is the dominant below-cloud process. A small part of the samples is  
573 distributed in the first and second quadrant, and their  $\Delta\delta$  are close to 0‰ while  $\Delta d$  are  
574 a little higher than 0‰. This cluster of samples implies that the below-cloud evaporation  
575 and cloud-based isotopic fractionation tend to achieve a complete equilibrium state.  
576 Interestingly, in our samples, most of the snow samples seize the third quadrant, which  
577 is suggestive of below-cloud evaporation with less impact on them, and their initial  
578 signal after cloud-based equilibrium fractionation is well retained. According to results  
579 from numerical simulations and in-situ observations, Graf et al. (2019) summarized



580 that raindrop size and precipitation intensity appear to be the important driving factors  
581 of the below-cloud processes, because raindrops with large diameter and high  
582 intensity will reduce their residence time in the atmospheric column, and lower the  
583 evaporation possibility during its way down toward the ground surface. However, as  
584 for snowfall events, it seems unreasonable to explain the strongly negative  $\Delta\delta$  from  
585 through the drop size and rain rate (Fig. 4). It is well known that snowfall events  
586 generally happen in low-temperature conditions, and correspond to weak evaporation,  
587 due to the lower diffusion speed of the ice phase to vapor as compared to liquid to  
588 vapor. Hence, rain/snow formed under such circumstances, its isotopic signals will not  
589 be largely changed by the environmental factors during its falling, which leads the  $\Delta\delta$   
590 to be more negative with the decrease of temperature, such as the phenomenon  
591 observed in Graf's et al. (2019) study during the post-frontal periods. Our results  
592 suggest that in addition drop size and rain rate, precipitation type is also an essential  
593 factor that needs to be fully considered in the below-cloud processes.



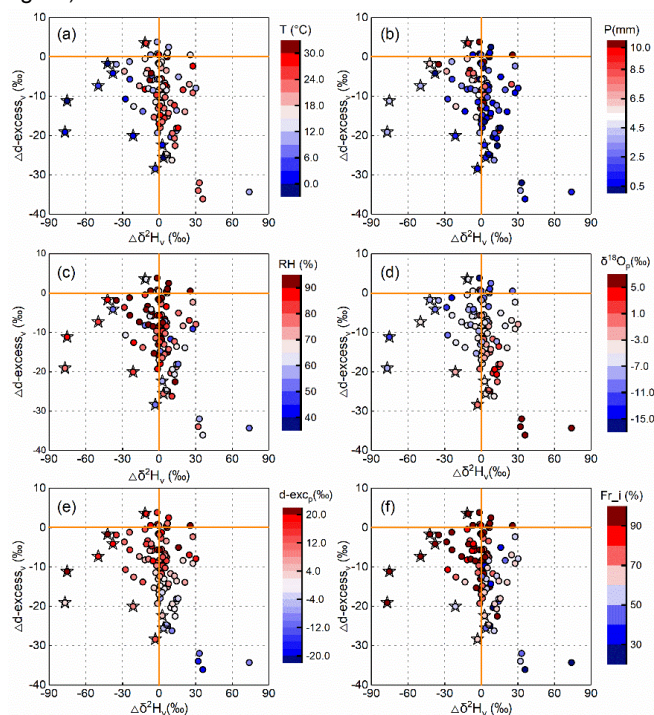
594 Figure 4 The projection of our data on Graf et al. (2019) suggested  $\Delta d\Delta\delta$ -diagram. The solid  
595 lines stand for  $\Delta d$ - $\text{excess}_v$  and  $\Delta\delta^2\text{H}_v$  of 0‰. The dashed line corresponds to the linear fit  
596 through the samples with the 95% confidence band in red shading.

597

598 Meteorological factors, such as precipitation amount, temperature, and RH, are the  
599 main factors affecting below-cloud evaporation (Li et al., 2016b; Peng et al., 2007),  
600 and have been well studied by combined with precipitation  $d$ - $\text{excess}_p$  (Ma et al., 2014;  
601 Wang et al., 2016b). In order to further analyze the below-cloud processes, we add the  
602 meteorological and isotopic information on the  $\Delta d\Delta\delta$ -diagram (Fig. 5). Generally, with



603 regard to high  $\Delta^2H_v$  samples, the corresponding meteorological condition is high  
604 temperature, low precipitation amount, and low RH (Fig. 5a-c). In contrast, under a  
605 condition of low air temperature, high RH, and large precipitation amount, the  $\Delta^2H_v$  of  
606 samples are relatively more negative (Fig. 5a-c). As below-cloud processes are  
607 controlled by multi-variable factors, it is hard to only use single physical variable to  
608 explain the below-cloud evaporation (Ma et al., 2014; Wang et al., 2016b). For example,  
609 under the highest temperature condition (two most red dots in Fig. 5a), the below-cloud  
610 evaporation effect should be higher, and cause  $\Delta^2H_v$  to be more positive and  $\Delta d$ -  
611 excess<sub>v</sub> to be more negative. However, under such circumstances, both the  $\Delta^2H_v$  and  
612  $\Delta d$ -excess<sub>v</sub> of the two samples are close to 0‰. By considering the precipitation  
613 amount, the two samples collected under the highest temperature condition are  
614 associated with a relatively larger precipitation amount which will temper the intensity of  
615 below-cloud evaporation. In addition, higher temperature corresponds to higher  
616 saturation vapor pressure, and a larger number of water molecules present in the  
617 atmosphere, which may enable substantial, rapid equilibration of water molecules  
618 between raindrops and ambient vapor during fall. Similarly, the samples with lower  
619 precipitation amount are associated with high RH, and cause the  $\Delta^2H$  distributed  
620 around 0‰. For the snow samples, the data with positive  $\Delta^2H$  is related to the very  
621 low RH (Fig. 5c).





622 Figure 5  $\Delta d/\Delta\delta$ -diagram for the precipitation samples with meteorological factors and  
623 precipitation isotopic information. Temperature (a); Precipitation amount (b); Relative humidity  
624 (c);  $\delta^{18}\text{O}_p$  of precipitation (d);  $d\text{-excess}_p$  of precipitation (e); Remaining fraction of evaporation  
625 (f). The dots with a star represent the snow samples.

626

627 In contrast to meteorological factors, the pattern of precipitation isotopic composition  
628 distribution on the  $\Delta d/\Delta\delta$ -diagram is more clear. Under the high below-cloud  
629 evaporation condition, the  $\delta^{18}\text{O}_p$  is more positive and  $d\text{-excess}_p$  is relatively negative  
630 (Fig. 5d and 5e). Correspondingly, the differences between equilibrated  $\delta^2\text{H}_{\text{eq-v}}$ ,  $d\text{-}$   
631  $\text{excess}_{\text{eq-v}}$  and observed  $\delta^2\text{H}_{\text{gr-v}}$ ,  $d\text{-excess}_{\text{gr-v}}$  are larger. Conversely, under low below-  
632 cloud evaporation conditions, mainly corresponding to the most snow samples, we  
633 could see the lowest  $\delta^{18}\text{O}_p$  and highest  $d\text{-excess}_p$  samples, respectively (Fig. 5d and  
634 5e). Moreover, the  $\Delta^2\text{H}_v$  is lower than 0‰ and  $\Delta d\text{-excess}_v$  is placed around 0‰.  
635 Basically, the  $\Delta d/\Delta\delta$ -diagram follows not only the traditional explanation that  $\Delta d < 0\text{‰}$   
636 and  $\Delta\delta > 0\text{‰}$  indicate the below-cloud evaporation process but also provides more  
637 information on the falling raindrops, such as  $\Delta d < 0\text{‰}$  and  $\Delta\delta < 0\text{‰}$  indicating the cloud  
638 signals, and  $\Delta d$  and  $\Delta\delta$  close to 0‰ indicating equilibrium conditions.

639

640 The slope of the regression line of  $\Delta d/\Delta\delta$  is -0.15 in our study (Fig. 4), which is half of  
641 the slope shown by Graf's et al. (2019). However, the slope of Graf's et al. (2019) is  
642 based on intra-event samples, while ours is on per-event samples, hence the two  
643 slopes cannot compare with each other directly. To advance the understanding of the  
644 slope, the controlling factors have been analyzed.

645

646 According to the sensitivity test by Graf et al. (2019), RH has a considerable impact on  
647 the slope of  $\Delta d/\Delta\delta$ . Low RH is coupled with more negative slopes, while the slopes of  
648  $\Delta d/\Delta\delta$  under high RH conditions are less negative or even positive (Fig. 5c). In addition,  
649 the temperature has a similar impact on the slopes of  $\Delta d/\Delta\delta$  as the RH (Fig. 5a). This  
650 indicates that the negative slopes of  $\Delta d/\Delta\delta$  correspond to a warm and dry environment.  
651 Besides, the slopes of  $\Delta d/\Delta\delta$  may relate to the precipitation types. When the samples  
652 are separated into rainfall and snowfall, the rainfall slope is -0.28 and the snowfall  
653 slope is only -0.12. Although the time scales are different in the two studies,  
654 interestingly, the slopes of rainfall are more close to each other. The slope of -0.3 could  
655 represent a general characteristic of rainfall for continental mid-latitude cold front  
656 passages (Graf et al., 2019), while the slope of snow samples is less negative in our  
657 study (Fig. S3). Certainly, to explore the relationship between the slope of  $\Delta d/\Delta\delta$  and  
658 the climatic characteristics and precipitation types, more validation works need to do



659 in future studies.

660

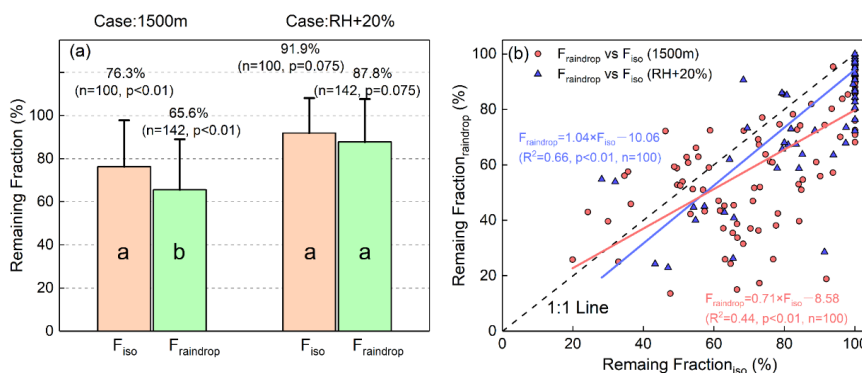
### 661 3.3 Comparing and analyzing the differences between $F_{\text{iso}}$ and $F_{\text{raindrop}}$

#### 662 3.3.1 The differences and reasons

663 In 1975, Stewart (1975) presented a set of empirical models, which is still widely used,  
664 to evaluate the below-cloud evaporation rate of the falling raindrop. However, Limited  
665 by measuring the cloud-based isotopic composition of the raindrop, many studies turn  
666 to use mass conservation model to evaluate the evaporation rate of the raindrop during  
667 its falling (Kong et al., 2013; Li et al., 2016a; Sun et al., 2020; Wang et al., 2016b).  
668 Here, for comparing their differences, we used the isotope method and mass  
669 conservation model to calculate the  $F_r$  after the below-cloud evaporation, respectively.  
670 For both methods, we only considered evaporative exchange in below-unsaturation  
671 cases. However, it is not true for the isotopic method, because both the evaporation  
672 and equilibration have effects on the  $\Delta\delta$  of the droplet during its falling from the cloud  
673 base. Here, we assumed that the below-cloud precipitation and surrounding ambient  
674 water vapor are in fully isotopic equilibrium, and  $F_{\text{iso}}$  only accounts for the evaporation  
675 effect on  $\Delta\delta$ . Therefore, the  $F_{\text{iso}}$  results may underestimate the remaining fraction of  
676 evaporation. To get the accurate  $F_{\text{iso}}$  results, more works need to do to partition the  
677 equilibration process from the evaporation in the future.

678

679 As shown in Fig. 6a, the computed mean of reaming fraction is 76.3% by the isotopic  
680 method ( $F_{\text{iso}}$ ), and 65.6% by the mass conservation model ( $F_{\text{raindrop}}$ ) based on two-year  
681 statistical results. The  $F_{\text{raindrop}}$  is statistically lower than the  $F_{\text{iso}}$  depending on the  
682 independent t-test ( $F=1.49$ ,  $p<0.01$ ). In addition, the  $F_{\text{iso}}$  and  $F_{\text{raindrop}}$  show an obvious  
683 difference, and that is the  $F_{\text{iso}}$  and  $F_{\text{raindrop}}$  seriously deviating from 1:1 line, when the  
684  $F_{\text{iso}}$  equals to 60%–80% (Fig. 6b). On a seasonal scale, the difference between  $F_{\text{iso}}$  and  
685  $F_{\text{raindrop}}$  in spring, summer, autumn, winter is 13.7%, 12.8%, 6.0%, and 25.0%,  
686 respectively, which is the largest in winter, and the lowest in autumn (Fig. 7).

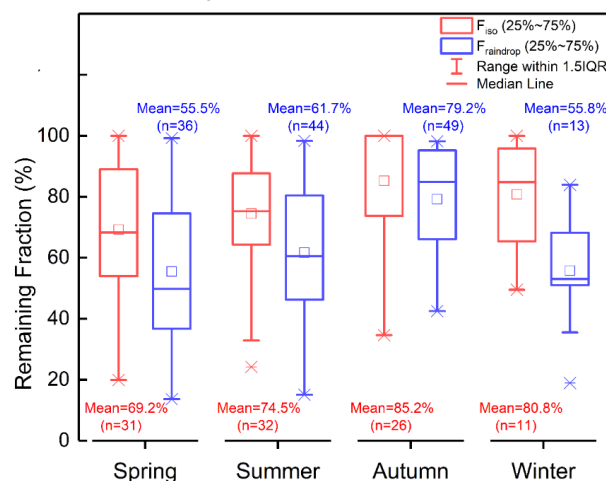




687 Figure 6 The comparison between the remaining fraction calculated by two methods. In (a), the  
688 taupe bars and the abbreviation of  $F_{iso}$  represent the remaining fraction calculated by the  
689 isotopic method, and the green bars and the abbreviation of  $F_{raindrop}$  represent the remaining  
690 fraction calculated by the mass conservation method. Case 1500m denotes that the raindrops  
691 evaporation calculation is based on the assumption of the cloud base at 1500m, and the  
692 raindrops are formed at that altitude. Case RH+20% denotes that based on the condition of  
693 case 1500m, we calculated the remaining fraction by increasing the ground observed RH by  
694 20%. n represents the number of samples used in statistics. The a and b in the bars denote the  
695 results of the independent t-test. In (b), the red dots represent the computed results of the  
696 remaining fraction under case 1500m condition, and the blue triangles represent the computed  
697 results under case RH+20% condition. The dash line is the 1:1 line.

698

699 To further explore the reason for the large differences by employing different methods,  
700 we performed the correlation analyses between meteorological factors and the  
701 remaining fraction of evaporation (Fig. S4). These analyses reveal that the most  
702 important impact factor both on  $F_{iso}$  and  $F_{raindrop}$  is RH (Fig. S4b). Although precipitation  
703 amounts have influences on  $F_{iso}$  and  $F_{raindrop}$  as well, their relationships are non-linear,  
704 and its effect on  $F_{iso}$  is rather weak ( $R^2=0.16$ , Fig. S4c). For temperature, no clear  
705 correlation was found. Wang et al. (2016b) explicitly pointed that among the  
706 parameters of temperature, precipitation amount, RH, and raindrop diameter, RH  
707 generally plays a decisive role on the obtained  $\Delta d$ -excess, which is positively  
708 correlated with the remaining fraction of raindrop.



709 Figure 7 Comparison between the mean remaining fraction results calculated by two methods  
710 in four seasons. n represent the number of samples used in statistics.

711

712 In order to analyze the underlying reason, first, we checked the equation used to  
713 calculate  $F_{iso}$  and  $F_{raindrop}$ . We noted that in both methods, RH is an important parameter  
714 to compute the remaining ratio. In the equation for computing  $F_{iso}$ , the values of  $\gamma$  and



715  $\beta$  are highly dependent on RH. Equally, in the  $F_{\text{raindrop}}$  computing equation, RH will be  
716 the decisive factor of evaporation intensity (E). Then, we tested the sensitivity between  
717  $\Delta\delta^{18}\text{O}$  and RH under different  $F_{\text{iso}}$  levels (Fig. S5). Our results showed, under high RH  
718 condition (60%~90%), a little variation of  $\Delta\delta^{18}\text{O}$  corresponded to a wide range of  $F_{\text{iso}}$   
719 distribution. We also noticed, under higher RH condition (above 90%), the simulated  
720  $\Delta\delta^{18}\text{O}$  is very small, normally lower than 0.5‰. However, in reality, the  $\Delta\delta^{18}\text{O}$  is  
721 generally greater than 0.5‰. Therefore, when the actual  $\Delta\delta^{18}\text{O}$  value is larger than the  
722 theoretical value, the calculated  $F_{\text{iso}}$  results will be larger than 100%, and this is in  
723 accordance with the actual condition. Because under higher RH condition, the raindrop  
724 evaporation ratio will decrease, and in turn the  $F_r$  will appropriately increase. Moreover,  
725 in the near-saturated air column, the raindrop is hardly evaporated.

726

727 Therefore, it is reasonable to assume that when the RH is higher, the difference  
728 between the  $F_{\text{iso}}$  and  $F_{\text{raindrop}}$  will be reduced. To validate our assumption, we computed  
729 the  $F_{\text{iso}}$  and  $F_{\text{raindrop}}$  by increasing RH by 20%, respectively. As expected, the mean  
730 annual difference was highly reduced, and statistically there is no significant difference  
731 (Fig. 6a, independent t-test,  $F=5.665$ ,  $p=0.075$ ). Moreover, the  $F_r$  computed by those  
732 two methods is closer to each other, while the correlation coefficient is highly increased,  
733 and the slope is closer to 1 (Fig. 6b). For the seasonal variations of  $F_r$ , the larger  
734 differences between  $F_{\text{iso}}$  and  $F_{\text{raindrop}}$  in spring and summer are regarding to the low RH  
735 in these seasons, while the small difference in autumn is related to the higher RH. For  
736 the largest difference in winter, it is most likely due to the fact that in the mass  
737 conservation model, the diameter of raindrop used to determine the terminal velocity  
738 of the raindrop ( $v_{\text{end}}$ ) and the evaporation intensity (E) do not account for snowfall factor  
739 resulting a great uncertainty in the calculation results.

740

### 741 3.3.2 Sensitivity test

742 In the below-cloud isotopic evaporation model (eq. 7), the two controlling factors are  
743 the equilibrium fractionation factor ( $\alpha$ ) and the RH. As the equilibrium fractionation  
744 factor varies with the cloud base altitude (mainly caused by the variation of  
745 temperature), we used the different altitudes to represent the variations of  $\alpha$ . In order  
746 to assess the relevance of different ambient conditions for the raindrop evaporation, a  
747 sensitivity test of  $F_r$  under different altitude and RH scenarios is exhibited in Fig. S6.  
748 With the increase of altitude, the  $F_r$  is gradually decreased. It is well known that with  
749 the increase of altitude, the raindrop falling distance will increase, and correspondingly  
750 the falling time will be extended. As a result, more fraction of raindrops would be



751 evaporated in the unsaturated atmospheric columns. When the RH increases by 20%,  
752 the atmospheric columns is near saturated, and largely decrease the evaporation  
753 possibility of falling raindrops. Conversely, the decrease of RH will strongly increase  
754 the evaporation proportion of falling raindrops. In addition, according to Fig. S6, the  $F_r$   
755 seems to be more sensitive to the changing of RH than that of altitude.

756

757 Comparing with the isotopic method, there are many parameters in the mass  
758 conservation model, such as raindrop diameter, evaporation intensity, raindrop falling  
759 velocity, resulting in the remaining fraction calculated by the mass conservation model  
760 with larger uncertainty. Taking the  $F_{iso}$  results as the benchmark, in our study, the mass  
761 conservation method will overestimate the raindrop evaporation ratios. The  
762 overestimation may be related to the low RH in our studying location. If we increase  
763 the RH by 20%, there is no significant difference between the two methods. This  
764 indicates that in high RH areas, either method could be used to calculate the  $F_r$ .  
765 However, in those arid and semi-arid areas, where the RH is relatively low, and the  
766 high latitude regions, where snowfall is frequent in winter, we need to cautiously use  
767 the result computed by the mass conservation method. Furthermore, Graf et al (2019)  
768 emphasized the role of the temperature structure, in particular melting layer height in  
769 the influence on the below-cloud processes, that a higher melting layer height prolongs  
770 the time for exchange between vapor and rain and leads to stronger equilibration and  
771 evaporation. In the future, it is therefore promising to study the raindrop formation  
772 heights, temperature profiles (e.g. melting layer heights), and atmospheric water vapor  
773 isotopic profiles when considering the below-cloud processes of the raindrops.

774

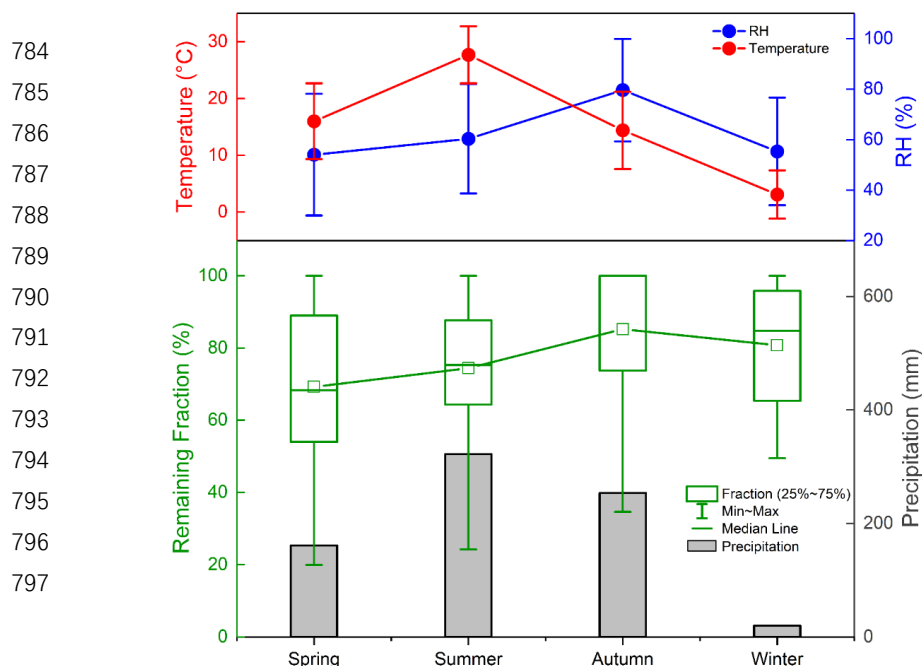
### 775 **3.4 The characteristics of below-cloud evaporation of raindrop in Xi'an**

776 As the phenomenon of below-cloud evaporation is very common in arid and semi-arid  
777 regions, to explore the information contained in the precipitation isotopic composition,  
778 it is important to clearly know that how much of the raindrops have been evaporated  
779 before they land on the ground. Here, we summarized the seasonal variations of  $F_{iso}$   
780 in Xi'an (Fig. 8).

781

782

783



798 Figure 8 The variations of temperature, relative humidity, precipitation amount and mean  
799 remaining fraction of evaporated raindrops in four seasons in Xi'an

800

801 By seasonally dividing the precipitation isotopic composition on the  $\Delta d\Delta\delta$ -diagram, it  
802 showed that samples collected in spring and summer dominate the evaporation phase,  
803 reflecting a stronger evaporation influence, while most of the winter precipitation and  
804 part of autumn precipitation monopolize the cloud signal phase indicating a weak or  
805 no below-cloud evaporation on these samples (Fig. S7). In addition, part of the autumn  
806 samples, of which the below-cloud evaporation and cloud-based isotopic exchange  
807 tends to achieve a complete equilibrium state is distributed in the equilibration phase  
808 (Fig. S7).

809

810 The mean raindrop evaporation rate is highest in spring and lowest in autumn based  
811 on two-year data (Fig. 8). The seasonal variation of  $F_{iso}$  basically followed the trend of  
812 seasonal variation of RH. Although the precipitation amount is highest in the summer,  
813 the temperature is extremely high and RH is relatively low, which causes the high  
814 evaporation rate in summer. In winter, the low evaporation rate may be related to the  
815 precipitation type, because snowfall is the main deposition type in this season.

816

#### 817 4 Conclusions

818 The below-cloud processes of precipitation are complex, variable, and influenced by



819 many factors, especially in the arid and semi-arid regions. Previously, below-cloud  
820 evaporation is the most well-studied post-condensation process with the aid of the  
821 slope of LMWL and d-excess of precipitation. In comparison, other below-cloud  
822 processes, such as the equilibration between the raindrop and ambient vapor, have  
823 paid less attention in different rain types. In this study, based on the two-year  
824 precipitation data collected in Xi'an, we systematically analyze its below-cloud  
825 processes, and get the following main conclusions:

826 1. In Xi'an, the precipitation isotopic signals mainly record the information of water  
827 vapor isotopic composition, but the signals could be changed by the below-cloud  
828 evaporation effect. This reminds us to be cautious in using precipitation isotopic  
829 compositions to study the hydrological cycle and climate changes in the arid and semi-  
830 arid regions.

831 2. Our work validates the general applicability of the  $\Delta d/\Delta \delta$ -diagram. Although there is  
832 a difference in timescale between Graf's et al. (2019) study (intra-event) and ours (per-  
833 event), by presenting our per-event precipitation isotopic results on the  $\Delta d/\Delta \delta$ -diagram,  
834 the below-cloud processes and their effects on the isotopic composition of vapor and  
835 precipitation can be clearly visualized. In Xi'an, the below-cloud evaporation is the main  
836 process during the raindrops falling. Snowfall samples are less influenced by the  
837 below-cloud processes and preserve their initial water vapor information. Hence, our  
838 results strengthen the reliability of using ice core to reconstruct the paleoclimate,  
839 paleoenvironment, and paleohydrology in the cold area. The different  $\Delta d/\Delta \delta$  slopes of  
840 rainfall and snowfall may be related to the precipitation types.

841 3. Compared with the isotopic method, the evaporation rate computed by the mass  
842 conservation model is overestimated. The relative humidity is the main controlling  
843 factor in computing the remaining fraction of raindrops below-cloud evaporation. Due  
844 to more uncertain parameters in the mass conservation model, such as raindrop  
845 diameter, evaporation intensity, raindrop falling velocity, and no consideration of  
846 precipitation type, it is more suitable to use the isotopic model to calculate the  
847 remaining fraction of evaporated raindrops.

848 4. In Xi'an, the evaporation rates are higher in spring and summer, and lower in autumn  
849 and winter, and this is related to the variation of local RH.

850  
851  
852  
853  
854



855 **Data availability**

856 The datasets can be obtained from the TableS1.

857

858 **Author contribution**

859 Meng Xing and Weiguo Liu designed the experiments, interpreted the results, and  
860 prepared the manuscript with contributions from all co-authors. Meng Xing and Jing  
861 Hu analyzed the precipitation and water vapor samples. Jing Hu maintained the  
862 experimental instruments.

863

864 **Competing interests**

865 The authors declare that they have no conflict of interest.

866

867

868 **Acknowledgment**

869 This work was supported by Science Foundation of China (No. 42177093), West Light  
870 Foundation of The Chinese Academy of Sciences, and China scholarship council. The  
871 authors would like to thank Mr. Xijing Cao for helping to collect precipitation samples.

872

873 **References**

874 Aemisegger, F., Sturm, P., Graf, P., Sodemann, H., Pfahl, S., Knohl, A. and Wernli, H.:  
875 Measuring variations of  $\delta$  18O and  $\delta$  2H in atmospheric water vapour using two commercial  
876 laser-based spectrometers: An instrument characterisation study, *Atmos. Meas. Tech.*, 5(7),  
877 1491–1511, doi:10.5194/amt-5-1491-2012, 2012.

878 Aemisegger, F., Spiegel, J. K., Pfahl, S., Sodemann, H., Eugster, W. and Wernli, H.: Isotope  
879 meteorology of cold front passages: A case study combining observations and modeling,  
880 *Geophys. Res. Lett.*, 42(13), 5652–5660, doi:10.1002/2015GL063988, 2015.

881 Bastrikov, V., Steen-Larsen, H. C., Masson-Delmotte, V., Gribanov, K., Cattani, O., Jouzel, J.  
882 and Zakharov, V.: Continuous measurements of atmospheric water vapour isotopes in western  
883 Siberia (Kourovka), *Atmos. Meas. Tech.*, 7(6), 1763–1776, doi:10.5194/amt-7-1763-2014,  
884 2014.

885 Benetti, M., Reverdin, G., Pierre, C., Merlivat, L., Risi, C., Steen-Larsen, H. C. and Vimeux, F.:  
886 Deuterium excess in marine water vapor: Dependency on relative humidity and surface wind  
887 speed during evaporation, *J. Geophys. Res.*, 119(2), 584–593, doi:10.1002/2013JD020535,  
888 2014.

889 Bowen, G. J., Cai, Z., Fiorella, R. P. and Putman, A. L.: Isotopes in the Water Cycle: Regional-  
890 to Global-Scale Patterns and Applications, *Annu. Rev. Earth Planet. Sci.*, 47(1), 453–479,  
891 doi:10.1146/annurev-earth-053018-060220, 2019.



- 892 Cai, Y., Cheng, H., An, Z., Edwards, R. L., Wang, X., Tan, L. and Wang, J.: Large variations of  
893 oxygen isotopes in precipitation over south-central Tibet during Marine Isotope Stage 5,  
894 *Geology*, 38(3), 243–246, doi:10.1130/G30306.1, 2010.
- 895 Chakraborty, S., Sinha, N., Chattopadhyay, R., Sengupta, S., Mohan, P. M. and Datye, A.:  
896 Atmospheric controls on the precipitation isotopes over the Andaman Islands, Bay of Bengal,  
897 *Sci. Rep.*, 6, 19555 [online] Available from: <https://doi.org/10.1038/srep19555>, 2016.
- 898 Christner, E., Aemisegger, F., Pfahl, S., Werner, M., Cauquoin, A., Schneider, M., Hase, F.,  
899 Barthlott, S. and Schädler, G.: The Climatological Impacts of Continental Surface Evaporation,  
900 Rainout, and Subcloud Processes on  $\delta D$  of Water Vapor and Precipitation in Europe, *J.*  
901 *Geophys. Res. Atmos.*, 123(8), 4390–4409, doi:10.1002/2017JD027260, 2018.
- 902 Clark, I. D. and Fritz, P.: *Environmental Isotopes in Hydrogeology*, Lewis, Boca Raton, Florida.,  
903 1997.
- 904 Conroy, J. L., Noone, D., Cobb, K. M., Moerman, J. W. and Konecky, B. L.: Paired stable  
905 isotopologues in precipitation and vapor: A case study of the amount effect within western  
906 tropical Pacific storms, *J. Geophys. Res. Atmos.*, 121(7), 3290–3303,  
907 doi:10.1002/2015JD023844, 2016.
- 908 Craig, H.: Isotopic Variations in Meteoric Waters, *Science* (80-. ), 133(3465), 1702–1703, 1961.
- 909 Dansgaard, W.: Stable isotopes in precipitation, *Tellus*, 16(4), 436–468,  
910 doi:10.3402/tellusa.v16i4.8993, 1964.
- 911 Deshpande, R. D., Maurya, A. S., Kumar, B., Sarkar, A. and Gupta, S. K.: Rain-vapor  
912 interaction and vapor source identification using stable isotopes from semiarid western India, *J.*  
913 *Geophys. Res. Atmos.*, 115(23), 1–11, doi:10.1029/2010JD014458, 2010.
- 914 Ellehoj, M. D., Steen-Larsen, H. C., Johnsen, S. J. and Madsen, M. B.: Ice-vapor equilibrium  
915 fractionation factor of hydrogen and oxygen isotopes: experimental investigations and  
916 implications for stable water isotope studies, *Rapid Commun. Mass Spectrom. Rcm*, 27(19),  
917 2149–2158, 2013.
- 918 Fiorella, R. P., Bares, R., Lin, J. C., Ehleringer, J. R. and Bowen, G. J.: Detection and variability  
919 of combustion-derived vapor in an urban basin, *Atmos. Chem. Phys.*, 18(12), 8529–8547,  
920 doi:10.5194/acp-18-8529-2018, 2018.
- 921 FISHER, D. A.: Remarks on the deuterium excess in precipitation in cold regions, *Tellus B*,  
922 43(5), 401–407, doi:<https://doi.org/10.1034/j.1600-0889.1991.t01-4-00006.x>, 1991.
- 923 Froehlich, K., Kralik, M., Papesch, W., Rank, D., Scheifinger, H. and Stichler, W.: Deuterium  
924 excess in precipitation of Alpine regions – moisture recycling, *Isotopes Environ. Health Stud.*,  
925 44(1), 61–70, doi:10.1080/10256010801887208, 2008.
- 926 Gat, J. R.: OXYGEN AND HYDROGEN ISOTOPES IN THE HYDROLOGIC CYCLE, *Annu.*  
927 *Rev. Earth Planet. Sci.*, 24(1), 225–262, doi:10.1146/annurev.earth.24.1.225, 1996.
- 928 Gorski, G., Strong, C., Good, S. P., Bares, R., Ehleringer, J. R. and Bowen, G. J.: Vapor  
929 hydrogen and oxygen isotopes reflect water of combustion in the urban atmosphere, *Proc. Natl.*  
930 *Acad. Sci.*, 112(11), 3247–3252, doi:10.1073/pnas.1424728112, 2015.
- 931 Graf, P., Wernli, H., Pfahl, S. and Sodemann, H.: A new interpretative framework for below-



- 932 cloud effects on stable water isotopes in vapour and rain, *Atmos. Chem. Phys.*, 19(2), 747–765,  
933 doi:10.5194/acp-19-747-2019, 2019.
- 934 Griffis, T. J., Wood, J. D., Baker, J. M., Lee, X., Xiao, K., Chen, Z., Welp, L. R., Schultz, N. M.,  
935 Gorski, G., Chen, M. and Nieber, J.: Investigating the source, transport, and isotope  
936 composition of water vapor in the planetary boundary layer, *Atmos. Chem. Phys.*, 16(8), 5139–  
937 5157, doi:10.5194/acp-16-5139-2016, 2016.
- 938 Guan, H., Zhang, X., Skrzypek, G., Sun, Z. and Xu, X.: Deuterium excess variations of rainfall  
939 events in a coastal area of south Australia and its relationship with synoptic weather systems  
940 and atmospheric moisture sources, *J. Geophys. Res. Atmos.*, 118(2), 1123–1138,  
941 doi:10.1002/jgrd.50137, 2013.
- 942 Horita, J. and Wesolowski, D. J.: Liquid-vapor fractionation of oxygen and hydrogen isotopes  
943 of water from the freezing to the critical temperature, *Geochim. Cosmochim. Acta*, 58(16),  
944 3425–3437, 1994.
- 945 Jacob, H. and Sonntag, C.: An 8-year record of the seasonal variation of 2 H and 18 O in  
946 atmospheric water vapour and precipitation at Heidelberg, Germany, *Tellus B Chem. Phys.*  
947 *Meteorol.*, 43(3), 291–300, doi:10.3402/tellusb.v43i3.15276, 1991.
- 948 Jeelani, G., Deshpande, R. D., Galkowski, M. and Rozanski, K.: Isotopic composition of daily  
949 precipitation along the southern foothills of the Himalayas: Impact of marine and continental  
950 sources of atmospheric moisture, *Atmos. Chem. Phys.*, 18(12), 8789–8805, doi:10.5194/acp-  
951 18-8789-2018, 2018.
- 952 Jouzel, J., Delaygue, G., Landais, A., Masson-Delmotte, V., Risi, C. and Vimeux, F.: Water  
953 isotopes as tools to document oceanic sources of precipitation, *Water Resour. Res.*, 49(11),  
954 7469–7486, doi:https://doi.org/10.1002/2013WR013508, 2013.
- 955 Kong, Y., Pang, Z. and Froehlich, K.: Quantifying recycled moisture fraction in precipitation of  
956 an arid region using deuterium excess. *Tellus Series B Chem Phys Meteorol Quantifying*  
957 *recycled moisture fraction in precipitation of an arid region using deuterium excess*, *Tellus B*,  
958 65(August 2015), 1–8, doi:10.3402/tellusb.v65i0.19251, 2013.
- 959 Laskar, A. H., Huang, J. C., Hsu, S. C., Bhattacharya, S. K., Wang, C. H. and Liang, M. C.:  
960 Stable isotopic composition of near surface atmospheric water vapor and rain-vapor interaction  
961 in Taipei, Taiwan, *J. Hydrol.*, 519(PB), 2091–2100, doi:10.1016/j.jhydrol.2014.10.017, 2014.
- 962 Li, L. and Garzzone, C. N.: Spatial distribution and controlling factors of stable isotopes in  
963 meteoric waters on the Tibetan Plateau: Implications for paleoelevation reconstruction, *Earth*  
964 *Planet. Sci. Lett.*, 460, 302–314, doi:10.1016/j.epsl.2016.11.046, 2017.
- 965 Li, Z., Qi, F., Wang, Q. J., Kong, Y., Cheng, A., Song, Y., Li, Y., Li, J. and Guo, X.: Contributions  
966 of local terrestrial evaporation and transpiration to precipitation using  $\delta$  18 O and D-excess as  
967 a proxy in Shiyang inland river basin in China, *Glob. Planet. Chang.*, 146, 140–151, 2016a.
- 968 Li, Z., Feng, Q., Wang, Y., Li, J., Guo, X. and Li, Y.: Effect of sub-cloud evaporation on the  $\delta$   
969 18 O of precipitation in Qilian Mountains and Hexi Corridor, China, *Sci. Cold Arid Reg.*, 8(5),  
970 378–387, doi:10.3724/SP.J.1226.2016.00378.Effect, 2016b.
- 971 Liu, W., Feng, X., Liu, Y., Zhang, Q. and An, Z.:  $\delta$ 18O values of tree rings as a proxy of monsoon



- 972 precipitation in arid Northwest China, *Chem. Geol.*, 206(1), 73–80,  
973 doi:https://doi.org/10.1016/j.chemgeo.2004.01.010, 2004.
- 974 Liu, W., Liu, H., Wang, Z., An, Z. and Cao, Y.: Hydrogen isotopic compositions of long-chain  
975 leaf wax n-alkanes in Lake Qinghai sediments record palaeohydrological variations during the  
976 past 12 ka, *Quat. Int.*, 449, 67–74, doi:https://doi.org/10.1016/j.quaint.2017.05.024, 2017a.
- 977 Liu, W., Wang, H., Leng, Q., Liu, H., Zhang, H. and Xing, M.: Hydrogen isotopic compositions  
978 along a precipitation gradient of Chinese Loess Plateau: Critical roles of precipitation /  
979 evaporation and vegetation change as controls for leaf wax  $\delta$  D, *Chem. Geol.*, 528(April),  
980 119278, doi:10.1016/j.chemgeo.2019.119278, 2019.
- 981 Liu, Y., Liu, H., Song, H., Li, Q., Burr, G. S., Wang, L. and Hu, S.: A monsoon-related 174-year  
982 relative humidity record from tree-ring  $\delta$ 18O in the Yaoshan region, eastern central China, *Sci.*  
983 *Total Environ.*, 593–594, 523–534, doi:https://doi.org/10.1016/j.scitotenv.2017.03.198, 2017b.
- 984 Ma, Q., Zhang, M., Wang, S., Wang, Q., Liu, W., Li, F. and Chen, F.: An investigation of  
985 moisture sources and secondary evaporation in Lanzhou, Northwest China, *Environ. Earth Sci.*,  
986 71(8), 3375–3385, doi:10.1007/s12665-013-2728-x, 2014.
- 987 Merlivat, L. and Jouzel, J.: Global climatic interpretation of the deuterium-oxygen 18 relationship  
988 for precipitation, *J. Geophys. Res. Ocean.*, 84(C8), 5029–5033,  
989 doi:https://doi.org/10.1029/JC084iC08p05029, 1979.
- 990 Müller, S., Stumpp, C., Sørensen, J. H. and Jessen, S.: Spatiotemporal variation of stable  
991 isotopic composition in precipitation: Post-condensational effects in a humid area, *Hydrol.*  
992 *Process.*, 31(18), 3146–3159, doi:10.1002/hyp.11186, 2017.
- 993 Noone, D., Risi, C., Bailey, A., Berkelhammer, M., Brown, D. P., Buening, N., Gregory, S.,  
994 Nusbaumer, J., Schneider, D., Sykes, J., Vanderwende, B., Wong, J., Meillier, Y. and Wolfe,  
995 D.: Determining water sources in the boundary layer from tall tower profiles of water vapor and  
996 surface water isotope ratios after a snowstorm in Colorado, *Atmos. Chem. Phys.*, 13(3), 1607–  
997 1623, doi:10.5194/acp-13-1607-2013, 2013.
- 998 Peng, H., Mayer, B., Harris, S. and Krouse, H. R.: The influence of below-cloud secondary  
999 effects on the stable isotope composition of hydrogen and oxygen in precipitation at Calgary,  
1000 Alberta, Canada, *Tellus, Ser. B Chem. Phys. Meteorol.*, 59(4), 698–704, doi:10.1111/j.1600-  
1001 0889.2007.00291.x, 2007.
- 1002 Peng, T. R., Liu, K. K., Wang, C. H. and Chuang, K. H.: A water isotope approach to assessing  
1003 moisture recycling in the island-based precipitation of Taiwan: A case study in the western  
1004 Pacific, *Water Resour. Res.*, 47(8), 1–11, doi:10.1029/2010WR009890, 2011.
- 1005 Putman, A. L., Fiorella, R. P., Bowen, G. J. and Cai, Z.: A Global Perspective on Local Meteoric  
1006 Water Lines-SM, *Water Resour. Res.*, 1–6, doi:10.1351/pac198961081483.Jaffey, 2019a.
- 1007 Putman, A. L., Fiorella, R. P., Bowen, G. J. and Cai, Z.: A Global Perspective on Local Meteoric  
1008 Water Lines: Meta-analytic Insight into Fundamental Controls and Practical Constraints, *Water*  
1009 *Resour. Res.*, 2019WR025181, doi:10.1029/2019WR025181, 2019b.
- 1010 Rangarajan, R., Laskar, A. H., Bhattacharya, S. K., Shen, C. C. and Liang, M. C.: An insight  
1011 into the western Pacific wintertime moisture sources using dual water vapor isotopes, *J. Hydrol.*,



- 1012 547, 111–123, doi:10.1016/j.jhydrol.2017.01.047, 2017.
- 1013 Salamalikis, V., Argiriou, A. A. and Dotsika, E.: Isotopic modeling of the sub-cloud evaporation  
1014 effect in precipitation, *Sci. Total Environ.*, 544, 1059–1072, doi:10.1016/j.scitotenv.2015.11.072,  
1015 2016.
- 1016 Salmon, O. E., Welp, L. R., Baldwin, M., Hajny, K., Stirm, B. H. and Shepson, P. B.: Vertical  
1017 profile observations of water vapor deuterium excess in the lower troposphere, *Atmos. Chem.*  
1018 *Phys. Discuss.*, (January), 1–35, doi:10.5194/acp-2018-1313, 2019.
- 1019 Spiegel, J. K., Aemisegger, F., Scholl, M., Wienhold, F. G., Collett, J. L., Lee, T., Van Pinxteren,  
1020 D., Mertes, S., Tilgner, A., Herrmann, H., Werner, R. A., Buchmann, N. and Eugster, W.: Stable  
1021 water isotopologue ratios in fog and cloud droplets of liquid clouds are not size-dependent,  
1022 *Atmos. Chem. Phys.*, 12(20), 9855–9863, doi:10.5194/acp-12-9855-2012, 2012a.
- 1023 Spiegel, J. K., Aemisegger, F., Scholl, M., Wienhold, F. G., Collett, J. L., Lee, T., Van Pinxteren,  
1024 D., Mertes, S., Tilgner, A., Herrmann, H., Werner, R. A., Buchmann, N. and Eugster, W.:  
1025 Temporal evolution of stable water isotopologues in cloud droplets in a hill cap cloud in central  
1026 Europe (HCCT-2010), *Atmos. Chem. Phys.*, 12(23), 11679–11694, doi:10.5194/acp-12-11679-  
1027 2012, 2012b.
- 1028 Steen-Larsen, H. C., Johnsen, S. J., Masson-Delmotte, V., Stenni, B., Risi, C., Sodemann, H.,  
1029 Balslev-Clausen, D., Blunier, T., Dahl-Jensen, D., Ellehøj, M. D., Falourd, S., Grindsted, A.,  
1030 Gkinis, V., Jouzel, J., Popp, T., Sheldon, S., Simonsen, S. B., Sjolte, J., Steffensen, J. P.,  
1031 Sperlich, P., Sveinbjörnsdóttir, A. E., Vinther, B. M. and White, J. W. C.: Continuous monitoring  
1032 of summer surface water vapor isotopic composition above the Greenland Ice Sheet, *Atmos.*  
1033 *Chem. Phys.*, 13(9), 4815–4828, doi:10.5194/acp-13-4815-2013, 2013.
- 1034 Stewart, M. K.: Stable isotope fractionation due to evaporation and isotopic exchange of falling  
1035 waterdrops: Applications to atmospheric processes and evaporation of lakes, *J. Geophys. Res.*,  
1036 80(9), 1133–1146, doi:10.1029/JC080i009p01133, 1975.
- 1037 Sun, C., Chen, Y., Li, J., Chen, W. and Li, X.: Stable isotope variations in precipitation in the  
1038 northwesternmost Tibetan Plateau related to various meteorological controlling factors, *Atmos.*  
1039 *Res.*, 227(April), 66–78, doi:10.1016/j.atmosres.2019.04.026, 2019.
- 1040 Sun, C., Chen, W., Chen, Y. and Cai, Z.: Stable isotopes of atmospheric precipitation and its  
1041 environmental drivers in the Eastern Chinese Loess Plateau, China, *J. Hydrol.*, 581(November  
1042 2019), 124404, doi:10.1016/j.jhydrol.2019.124404, 2020.
- 1043 Tan, L., An, Z., Huh, C.-A., Cai, Y., Shen, C.-C., Shiao, L.-J., Yan, L., Cheng, H. and Edwards,  
1044 R. L.: Cyclic precipitation variation on the western Loess Plateau of China during the past four  
1045 centuries, *Sci. Rep.*, 4(1), 6381, doi:10.1038/srep06381, 2014.
- 1046 Thompson, L. G., Yao, T., Mosley-Thompson, E., Davis, M. E., Henderson, K. A. and Lin, P.-  
1047 N.: A High-Resolution Millennial Record of the South Asian Monsoon from Himalayan Ice Cores,  
1048 *Science* (80-. ), 289(5486), 1916 LP – 1919, doi:10.1126/science.289.5486.1916, 2000.
- 1049 Tian, C., Wang, L., Kaseke, K. F. and Bird, B. W.: Stable isotope compositions ( $\delta^2\text{H}$ ,  $\delta^{18}\text{O}$   
1050 and  $\delta^{17}\text{O}$ ) of rainfall and snowfall in the central United States, *Sci. Rep.*, (October 2017), 1–  
1051 15, doi:10.1038/s41598-018-25102-7, 2018.



- 1052 Wan, H., Liu, W. and Xing, M.: Isotopic composition of atmospheric precipitation and its tracing  
1053 significance in the Laohequ Basin, Loess plateau, China, *Sci. Total Environ.*, 640–641(May),  
1054 989–996, doi:10.1016/j.scitotenv.2018.05.338, 2018.
- 1055 Wang, S., Zhang, M., Che, Y., Chen, F. and Fang, Q.: Contribution of recycled moisture to  
1056 precipitation in oases of arid central Asia: A stable isotope approach, *Water Resour. Res.*, 52(4),  
1057 3246–3257, doi:10.1002/2015WR018135, 2016a.
- 1058 Wang, S., Zhang, M., Che, Y., Zhu, X. and Liu, X.: Influence of Below-Cloud Evaporation on  
1059 Deuterium Excess in Precipitation of Arid Central Asia and Its Meteorological Controls, *J.*  
1060 *Hydrometeorol.*, 17(7), 1973–1984, doi:10.1175/JHM-D-15-0203.1, 2016b.
- 1061 Wang, S., Zhang, M., Hughes, C. E., Crawford, J., Wang, G., Chen, F., Du, M., Qiu, X. and  
1062 Zhou, S.: Meteoric water lines in arid Central Asia using event-based and monthly data, *J.*  
1063 *Hydrol.*, 562(May), 435–445, doi:10.1016/j.jhydrol.2018.05.034, 2018a.
- 1064 Wang, Z., An, Z., Liu, Z., Qiang, X., Zhang, F. and Liu, W.: Hydroclimatic variability in loess  
1065  $\delta D_{wax}$  records from the central Chinese Loess Plateau over the past 250 ka, *J. Asian Earth*  
1066 *Sci.*, 155, 49–57, doi:https://doi.org/10.1016/j.jseaes.2017.11.008, 2018b.
- 1067 Welp, L. R., Lee, X., Kim, K., Griffis, T. J., Billmark, K. A. and Baker, J. M.:  $\delta 18O$  of water  
1068 vapour, evapotranspiration and the sites of leaf water evaporation in a soybean canopy, *Plant,*  
1069 *Cell Environ.*, 31(9), 1214–1228, doi:10.1111/j.1365-3040.2008.01826.x, 2008.
- 1070 Wen, X. F., Zhang, S. C., Sun, X. M., Yu, G. R. and Lee, X.: Water vapor and precipitation  
1071 isotope ratios in Beijing, China, *J. Geophys. Res. Atmos.*, 115(1), 1–10,  
1072 doi:10.1029/2009JD012408, 2010.
- 1073 Wu, J., Li, P. and Qian, H.: Variation characteristics of meteorological elements and prediction  
1074 model of available precipitation in Xi'an city, *South-to-North water Transf. water Sci. Technol.*,  
1075 11(001), 50–54, 2013.
- 1076 Xing, M., Liu, W., Li, X., Zhou, W., Wang, Q., Tian, J., Li, X., Tie, X., Li, G., Cao, J., Bao, H. and  
1077 An, Z.: Vapor isotopic evidence for the worsening of winter air quality by anthropogenic  
1078 combustion-derived water, *Proc. Natl. Acad. Sci.*, 117(52), 33005–33010,  
1079 doi:10.1073/pnas.1922840117, 2020.
- 1080 Yao, T., Thompson, L. G., Mosley-Thompson, E., Zhihong, Y., Xingping, Z. and Lin, P.-N.:  
1081 Climatological significance of  $\delta 18O$  in north Tibetan ice cores, *J. Geophys. Res. Atmos.*,  
1082 101(D23), 29531–29537, doi:10.1029/96JD02683, 1996.
- 1083 Yao, T., Masson-Delmotte, V., Gao, J., Yu, W., Yang, X., Risi, C., Sturm, C., Werner, M., Zhao,  
1084 H., He, Y., Ren, W., Tian, L., Shi, C. and Hou, S.: A review of climatic controls on  $\delta 18O$  in  
1085 precipitation over the Tibetan Plateau: Observations and simulations, *Rev. Geophys.*, 51(4),  
1086 525–548, doi:10.1002/rog.20023, 2013.
- 1087 Zhang, M. and Wang, S.: A review of precipitation isotope studies in China: Basic pattern and  
1088 hydrological process, *J. Geogr. Sci.*, 26(7), 921–938 [online] Available from:  
1089 <http://www.geogsci.com>, 2016.
- 1090 Zhao, L., Liu, X., Wang, N., Kong, Y., Song, Y., He, Z., Liu, Q. and Wang, L.: Contribution of  
1091 recycled moisture to local precipitation in the inland Heihe River Basin, *Agric. For. Meteorol.*,



1092 271(July 2018), 316–335, doi:10.1016/j.agrformet.2019.03.014, 2019.  
1093 Zhu, G. F., Li, J. F., Shi, P. J., He, Y. Q., Cai, A., Tong, H. L., Liu, Y. F. and Yang, L.:  
1094 Relationship between sub-cloud secondary evaporation and stable isotope in precipitation in  
1095 different regions of China, Environ. Earth Sci., 75(10), 876, 2016.  
1096